Colloids and Surfaces A 592 (2020) 124576

Contents lists available at ScienceDirect

Colloids and Surfaces A

journal homepage: www.elsevier.com/locate/colsurfa

Particle-induced nanobubble generation for material-selective nanoparticle flotation

Vinzent Olszok[a,*], Juliana Rivas-Botero[a], Annett Wollmann[a], Bernd Benker[b], Alfred P. Weber[a]

[a] Clausthal University of Technology, Institute of Particle Technology, Leibnizstraße 19, 38678, Clausthal-Zellerfeld, Germany
[b] Clausthal University of Technology, Clausthal Institute of Environmental Technologies (CUTEC), Leibnizstraße 21+23, 38678, Clausthal-Zellerfeld, Germany

GRAPHICAL ABSTRACT

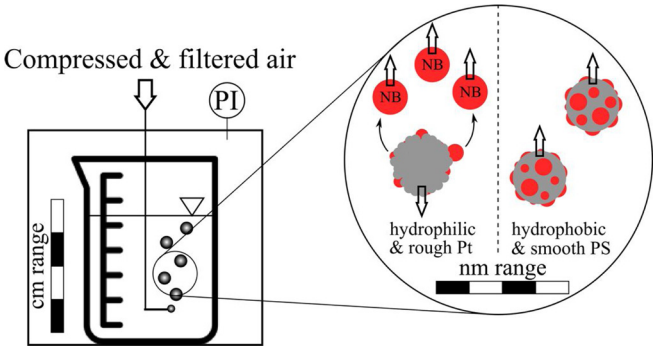

ARTICLE INFO

Keywords:
Nanobubbles
Flotation
Nanoparticle-tracking-analysis
Pressurization
Platinum nanoparticles
Polystyrene nanoparticles

ABSTRACT

The presented work investigates particle-induced nanobubble generation in order to extend the applicability of material-selective pressure flotation towards nanoscale materials. During a gas treatment procedure, filtered compressed air in the range of 0 bar–2 bar overpressure was introduced into colloidal suspensions in ultra-purified water until saturation was obtained. Nanobubble formation in the suspension occurred after slow depressurization with a gas vent. Suspensions of platinum nanoparticles and polystyrene beads were used to examine the effects of particle hydrophobicity and roughness. Using nanoparticle-tracking-analysis (NTA), the evaluation of particle size and scattered light intensity showed the occurrence of nanobubbles, both, as a separate phase (bulk nanobubbles) and attached to the particles' surface. The sharply separated nanobubble peak was observed in number density NTA plots of gas treated platinum nanoparticles. The size of the hydrophilic platinum particles remained unchanged. In contrast, for hydrophobic polystyrene particles, the hydrodynamic diameter increased during a gas treatment procedure. The experimental results are understood, on the one hand, as the nucleation of bulk nanobubbles in the cavities of hydrophilic platinum particles and, on the other, as surface-growth of nanobubbles attached to the hydrophobic polymer particles.

Abbreviations: NBs, Nanobubbles; Pt, Platinum; PS, Polystyrene; PSD, Particle size distribution; NTA, Nanoparticle-tracking-analysis; UPW, Ultra-purified water; TEM, Transmission electron microscope; MBs, Microbubbles; SSPS, Small-scale pressurization system; DLS, Dynamic light scattering; RMM, Resonant mass measurement method; SDS, Sodium dodecyl sulfate; Conc., Concentration; Mean int., Mean intensity; CPC, Condensation particle counter; SD, Standard deviation; AFM, Atomic force microscopy

* Corresponding author.
E-mail address: vinzent.olszok@tu-clausthal.de (V. Olszok).

https://doi.org/10.1016/j.colsurfa.2020.124576
Received 29 November 2019; Received in revised form 5 February 2020; Accepted 10 February 2020
Available online 10 February 2020

Nomenclature

C_N	Number concentration (# ml^{-1})
$C_{N,\ i}$	Number concentration in class i within a PSD (# ml^{-1})
D	Diffusion coefficient (m s^{-2})
d_{HD}	Hydrodynamic particle diameter (m)
$d_{HD,i}$	Hydrodynamic particle diameter of class i within a PSD (m)
d_i	Inner diameter (mm)
d_o	Outer diameter (mm)
i	Class within a PSD (-)
k_B	Boltzmann constant (J K^{-1})
n	Total number of classes i within a PSD (-)
N_{rep}	Number of replications (-)
p	Pressure (bar)
Q_0*	Cumulated particle concentration (# ml^{-1})
Q_3*	Cumulated particle volume (nm^3 ml^{-1})
T	Temperature (K)
t	Time (s)
$V_{N,i}$	Volume of particles in class i within a PSD (nm^3)
x, y	Coordinates (-)
η	Dynamic viscosity (Pa s)
λ	Wavelength (m)
$\tau_{1/2}$	Half-life of exponential pressure drop (s)

1. Introduction

During the last years, liquids containing gas bubbles in micro- and nanoscale range (microbubbles MBs and nanobubbles NBs) have been intensively investigated because of their special properties and wide range of applications. Next to investigations regarding the existence as well as the generation of bulk NBs created by different methods and gases [1–4], there is strong interest in surface-attached NBs since they open up new applications in process engineering. For example, cavitation bubbles in flotation, generated by ultrasonic waves, were found to increase the yield of flotation processes [5,6] although according to Falcon [7] the effect is limited to particles with sizes above a few micrometers. It has been demonstrated that the presence of NBs led to the flotation of model particle systems in micrometer range [8], additionally, the effective parameters of NBs in froth flotation were investigated [9]. It is assumed that surface-attached NBs modify the hydrodynamic properties of particles during a collision with macroscopic bubbles. However, for further flotation applications towards recovering material in a nanoscale range, the critical step is the attachment of bulk NBs to the particles' surface. Although high relative movement between particles and bubbles improves the yield of finer particles by increasing inertial forces [10], a flotation of nanoscale material is still unattainable.

In contrast to collision-based flotation, this work focusses on pressure (release) flotation, i.e. on particle surface-generated NBs rather than NBs re-attached to a surface. Bubble generation due to pressure reduction also occurs in ultrasonic and cavitation flotation mentioned above, but in both cases, there is a strong mechanical agitation. In our apparatus, however, there is no input of mechanical energy beyond a gentle bubble flow, which will be explained in detail. The growing NBs can remain on the particles' surface or detach from it, which then contributes to the production of bulk NBs. The mechanism assumed to be relevant for NB formation and growth is related to heterogeneous nucleation with nanoparticles' surface as nuclei for dissolved gas molecules [11–14]. For the intended application of our process to the sorting of different materials, the key question is how surface growth of sessile NBs depends on nanoparticle hydrophobicity and surface roughness. Here, platinum and polystyrene particle materials were used in model particle systems aiming at future separation processes of precious metals from, for example, electronic waste.

For an investigation of suspended nanoparticles, bulk NBs and surface-attached NBs, several measurement techniques like dynamic light scattering (DLS) and resonant mass measurement method (RMM) are commonly applied [2,4,15,16]. Since DLS is not able to resolve binary particle systems with almost the same diameter [17,18] and since RMM cannot distinguish between surface-attached and bulk NBs in a sample, more precise measuring techniques are necessary. The alternative that has been used in this work is the nanoparticle-tracking-analysis (NTA) coming up with the unique feature of measuring two particle properties at the same time: tracking of individual particles

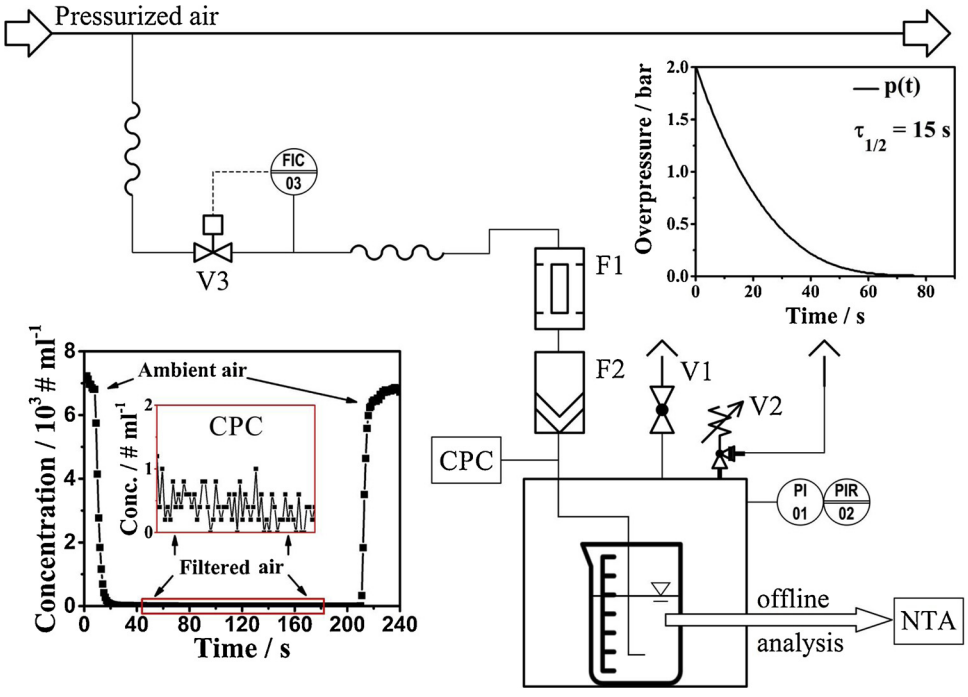

Fig. 1. Piping and instrumentation diagram of the small-scale pressurization system, F1 activated carbon filter, F2 particle filter, V1 needle valve, V2 relief valve, V3 mass flow controller, CPC: Condensation Particle Counter, NTA: Nanoparticle Tracking Analyzer. Inserts: Overpressure versus time with $\tau_{1/2}$ half-life of exponential pressure drop and concentration profile of CPC check-up of filtered air. The averaged absolute ambient pressure during the experiments was 950.2 mbar.

comes up with their mobility-equivalent size distribution and in parallel their scattering intensity recorded. The instrument can, therefore, distinguish between different kinds of particles of similar size. As described by Hu et al. [19] and Alheshibri et al. [20], for example, NTA is increasingly being used in characterization and detection of NBs. This trend shows the relevance in the analysis and detection of NBs and in combination with the multidimensional measurement of parameters, the NTA technique is considered to be extremely suitable for the investigations presented in this work.

2. Materials and methods

2.1. Bubble generator setup

A self-constructed small-scale pressurization system (SSPS) for approximately 50 ml of suspension was used as an NB generator (Fig. 1). Compressed air entered the SSPS through a mass flow controller (GSC-A9ST-BB22 Vögtlin Instruments GmbH) with pressures up to 10 bar and a constant flow rate of 2 liters per minute. Two inlet filters, an activated carbon filter, and a particle filter ensured contamination and particle-free gas stream into the SSPS cell and the sample, respectively (activated carbon element multifix FA06&FA11 RIEGLER & Co. KG, absolute filter DIF-BN-40 99,999 % Headline Filters GmbH). A check-up of the filtered air with a condensation particle counter (CPC, GRIMM Aerosol Technik Ainring GmbH & Co. KG, Model 5.403) proved a particle-free airflow into the pressure cell and liquid sample, respectively (CPC concentration profile as an insert in Fig. 1). The gas was bubbled through the liquid sample from a stainless steel tube (d_i = 1.5 mm, d_o = 3.0 mm).

After reaching the intended pressure in the SSPS-cell, the pressure was kept constant with a relief valve (SRV30 Hansun Engineering Co. LTD.) at a constant gas flow rate. In each batch, 50 ml of suspension were gas treated for 10 min at 0 bar, 1 bar and 2 bar overpressure. A gas pressure of 0 bar means in this context that saturation of the suspension with filtered air occurred at ambient pressure with the relief valve in wide-open position. There was no need for a depressurization step. This operation was carried out for pressure levels of 1 bar or 2 bar by opening a needle valve to a predefined position. Thus, in all experiments discussed in the following the pressure in the cell decayed in an exponential manner. This pressure release rate avoided any dynamic effects in the sample such as cavitation caused by ultrasonic or depressurization of a liquid sample through a valve. Uprising bubbles (e.g. MBs) did not induce any relevant shear stresses in the sample while cell depressurization, hence, dynamic effects are neglected for the conducted experiments. For an analysis of gas treated suspension, 5 ml of sample were taken for an offline measurement by NTA at ambient pressure after a gas treatment procedure. Thereby, an evaluation of NB-formation kinetics was not intended here.

2.2. Nanoparticle-tracking-analysis NTA

Investigations regarding the hydrodynamic diameter of both, particles and NBs were performed using a nanoparticle tracking analyzer (ZetaView® BASIC PMX-120 Particle Metrix GmbH). An NTA-device consists of a laser illuminating particles of a colloidal suspension within a flow-through measurement cell and a video camera system equipped with a microscopic lens. With ZetaView®, particles in a range from 10 nm up to 1000 nm can be detected depending on sample material and the used laser system [21]. The measurement cell including the sample was set to a constant temperature of 20 °C for all investigations reported. By detecting the Brownian diffusion of single particles in the suspension, nanoparticle-tracking-analysis determines the mean square displacement for those particles per time interval. Thus, during a single NTA measurement, hundreds to thousands of particles are tracked simultaneously to calculate a particle size distribution. From the analysis of the Brownian diffusion, which is measured here in two dimensions, the diffusion coefficient for a single particle can be calculated by Eq. (1). The Stokes-Einstein equation correlates the diffusion coefficient with the hydrodynamic particle diameter at a specific temperature and dynamic viscosity (Eq. (2)).

$$\langle x, y\rangle^2 = 4\,D\,t \tag{1}$$

$$D = \frac{k_B\,T}{3\,\pi\,\eta\,d_{HD}} \tag{2}$$

NTA also determines particle concentration (number based) of a sample from the total number of illuminated particles detected in the laser cross-section divided by the radiated volume (~3 nl) [21]. This evaluation, however, requires knowledge of the detection efficiency which must be provided from calibration experiments. For unknown samples or mixtures of known materials, the number concentration is only of relative use. Reproducible experiments under these conditions require strict procedures for the settings of all the optical parameters. For all NTA-measurements in this work, video camera settings like camera sensitivity (Sen) and camera shutter (Shu) were set to constant values, Sen = 80 % and Shu = 7.5 %.

Within the analyzed particle size range and the wavelength of the used NTA-laser (λ = 520 nm), *Rayleigh* scattering applies. *Rayleigh* scattering intensity depends on the relative complex refractive index, i.e. both, its scattering and absorption coefficient in relation to those of water. The quantitative effects of optical constants can be quite surprising since shiny metallic particles have a high absorption coefficient. By using NTA, information about the scattered light intensity of each tracked particle can be recorded additionally to particle size and concentration. Based on video raw data, a scattering intensity can be analyzed, averaged over the diffusive displacement (so-called “mean intensity”). In the following, however, particle brightness is used only in a qualitative manner to discriminate between nanoparticles and NBs. As mentioned before, different intensity per particle volume results in a material-dependent detection threshold and a counting efficiency. By using NTA, a particle size distribution and a mean intensity distribution can be measured in one single step.

In this work, particle size distributions (PSDs) are presented as particle number concentration (C_N) over hydrodynamic particle diameter (d_{HD}). The particle size of a species describes the diameter of a solid particle and an NB, respectively. In particle literature it is convenient to address "solid particles" and "fluid particles" (i.e. "drops" / "droplets" and "bubbles") all together as "particles". Scatterplots indicate for each particle the track-averaged scattered light intensity in arbitrary units versus particle size, with each tracked particle represented by a marker. All gas treatment experiments at a specific pressure were performed in five replications in order to obtain statistically verified results by means of NTA measurements. Thus, PSDs showing the mean values of particle diameter in each size class as calculated in terms of arithmetic average. Standard deviations are presented as error bars of particle concentration in PSDs plots below.

2.3. Medium

Ultra-purified water (UPW) at room temperature with constant electrical conductivity of 0.055 μS cm^{-1} was used for sample preparation and dilution. It was provided by an ultrapure water system (arium®pro UV TOC Sartorius AG) applying filtration through activated carbon and ion-exchange resin. UPW was degassed under vacuum for 20 min before use (pressure difference of 800 mbar to atmosphere).

Reference materials

The suspensions used in the experiments were prepared from commercially available particle size standards. Platinum particles (30 nm Platinum Nanoparticles Citrate NanoXact™ nanoComposix Inc.)

with a raspberry-like shape were used to provide a hydrophilic metallic particle surface. The undiluted standard was stabilized in 2 mmol l^{-1} aqueous citrate and the particles showed a hydrodynamic diameter of 39 nm [22]. A second hydrophilic particle material, spherical gold particles (30 nm Gold Nanospheres Citrate NanoXact™nanoComposix Inc.) with a smooth surface were also used for gas treatment experiments aiming at the influence of the particle surface morphology on NB production. Identical to Pt30 particles, Au30 was stabilized in 2 mmol l^{-1} aqueous citrate and displayed a hydrodynamic diameter of 38 nm [23].

Hydrophobic particle suspensions were prepared from a 70 nm mean diameter NIST-traceable polystyrene size standard (PS70 3070A Nanosphere™ Thermo Scientific Inc.). These polystyrene (PS) nanoparticles showed a smooth particle surface (see TEM micrographs Fig. 2). Pt30, PS70 and its binary mixture were used as main model systems for this work, while investigations with Au30 only supplemented the mentioned main model systems. Fig. 2 depicts the TEM micrographs, particle size distributions and scatterplots of Pt30 as hydrophilic particle material and PS70 as hydrophobic particle material. Information about Au30 is given in Fig. 5. Agglomerates in all these TEM micrographs are attributed solely to sample preparation.

In contrast to Pt30, PS70 particles were stabilized with an anionic surfactant, chemically similar to sodium dodecyl sulfate (SDS), to inhibit agglomeration in the undiluted suspension [24]. Despite dilution factors of 1000 for Pt30/Au30 and 250,000 for PS respectively, all suspensions were stable for the duration of the conducted tests as confirmed by NTA measurements of blank samples before and after each test series.

For gas treatment experiments of particle-free stabilizer solutions (named “citrate” and “SDS”), tri-sodium citrate dihydrate (p.a., Merck KGaA) and sodium dodecyl sulfate (70 % GC, Fluka Chemie AG) were used.

3. Results and discussion

3.1. Pressurization of ultra-purified water

The NTA measurement of gas treated UPW showed a low concentration of background particles or bubbles, whereas blank UPW appeared background-free. In the following, analyzed particles in gas treated UPW will be called NBs since other sources of contamination were carefully excluded.

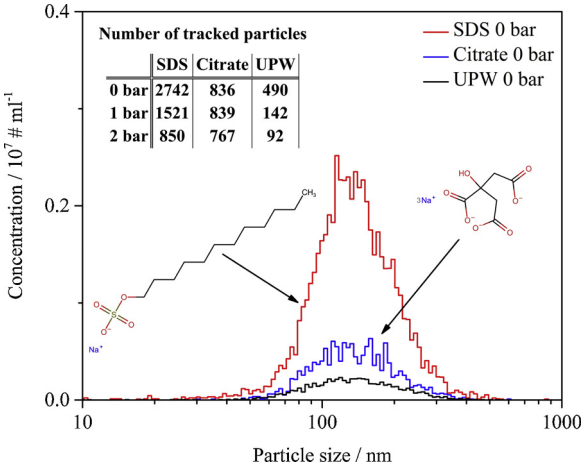

Fig. 3. Averaged PSDs (N_{rep} = 5) for gas treated sodium dodecyl sulfate solution (SDS), sodium citrate solution, and ultra-purified water (UPW) at ambient pressure. $C_{N,\ Peak\ SDS} = 2.5 \times 10^6$ # ml^{-1}, $C_{N,\ Peak\ Citrate} = 6.3 \times 10^5$ # ml^{-1}, $C_{N,\ Peak\ UPW} = 2.3 \times 10^5$ # ml^{-1}. Insert: Number of tracked particles after pressurization for background measurements and chemical structure of SDS and citrate.

NBs in a size range from 50 nm to 300 nm were found with a peak concentration of 2.3×10^5 # ml^{-1} for gas treatment at 0 bar (see UPW Fig. 3). The measured particle size distributions appeared consistent with investigations by Ushikubo et al. [4] who performed NB generation and NB stability experiments with NBs formed by a micro-bubble generator with pure oxygen and air. In our work, a higher gas pressure did not increase the number of generated bulk NBs after sample pressurization. In support of these results, Azevedo et al. [3], who investigated NBs in a surfactant-enriched aqueous system by forcing the gas-saturated liquid through a needle valve, detected a decreasing NB concentration at increasing pressure as well. Venting the SSPS after pressurization led to the formation of rising visible microbubbles (MBs)

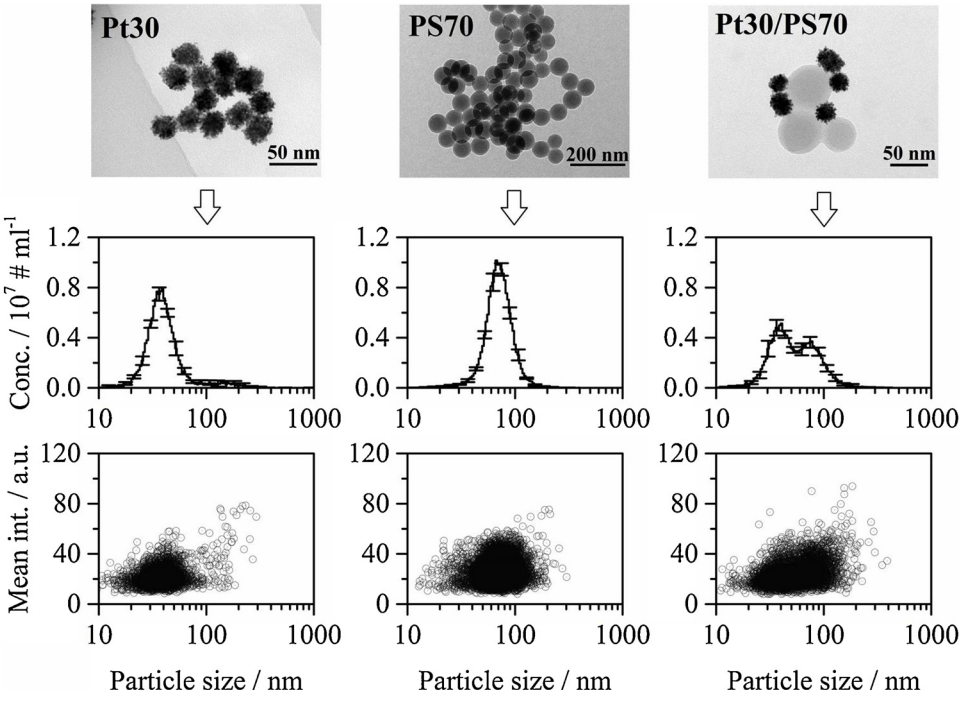

Fig. 2. TEM micrographs of platinum particles Pt30, polystyrene spheres PS70 and a binary mixture of both materials. Pt30 showed a rough and uneven surface with cavities, PS70 particles appeared perfectly spherical and presented a smooth surface morphology (first row of figures). Particle size distributions and scatterplots of blank diluted reference materials (second and third row of figures). Error bars in PSDs are given for every tenth size class, number of replications for error bars N_{rep} = 5.

while the pressure in the SSPS-cell slowly decreased. These MBs were presumably responsible for NBs being entrained from the suspension as described by Azevedo et al. [3].

In order to preclude stabilizer molecules like SDS for PS70 nanoparticles and sodium citrate for Pt30 nanoparticles respectively, from being responsible for NB formation, particle-free stabilizer solutions were gas treated and analyzed by NTA at a dilution typical for the conducted experiments. The results in Fig. 3 for ambient pressure showed significant production of bulk NBs, most of all with SDS. The hydrophobicity of the alkyl tail of SDS can be considered responsible for a NB nucleation while a citrate ion appears hydrophilic due to the spherically arranged charges. These experiments were repeated under pressure release conditions and showed a significantly lower NB production, which can be seen from a decreasing number of tracked particles at increased gas pressure (inserted table in Fig. 3). Thus, only PSDs at ambient pressure are given in Fig. 3. The mean particle sizes of NBs in samples at overpressure did not differ from those PSDs shown in Fig. 3 for ambient pressure. The amount of formed bulk NBs for UPW and citrate can be considered insignificant. The appearance of bulk NBs for gas treated SDS samples needs to be compared and discussed with experimental results for gas treated PS70 afterwards.

3.2. Pressurization of rough hydrophilic Pt30 particles

In contrast to the previous experiments (gas treatment of UPW Fig. 3), nanoscaled platinum particles (Pt30) present in the gas treated sample were able to enhance the formation of bulk NBs significantly which is shown by the appearance of a second peak in PSD for gas treated samples (Fig. 4). The blank Pt30 suspension showed a monomodal particle size distribution with a peak concentration of 8×10^6 # ml^{-1}. After gas treatment of Pt30 suspensions at ambient pressure, a bimodal particle size distribution appeared with a NB-concentration of approximately 2.7×10^6 # ml^{-1}. Compared to gas treated citrate solution at ambient pressure, the NB-concentration increased by a factor > 4. By raising the pressure up to 2 bar, the NBs in a size range from 70 nm to 200 nm remained constant in concentration while the Pt30 peak appeared to be constant in size.

As summarized in Fig. 9, the comparison of the calculated cumulative particle concentration Q_0* for Pt30 experiments showed an increase in total concentration for gas treated samples. Furthermore, under the assumption of spherical particles, the cumulative particle volume Q_3* (Fig. 10) increased nearly by a factor of five due to the appearance of a second, so-called NB peak at larger sizes. All presented data clearly indicated that both, in terms of number and volume, bulk NBs were generated due to the presence of Pt30 particles.

This conclusion is underlined by taking the scatterplots into consideration for the discussion (see inserts to Fig. 4). After gas treatment, a new cloud of large (about 70 nm–200 nm) bright signals appeared in the scatterplot. By comparison, the scatterplot representing the Pt30 particles experienced hardly any change. Since platinum is hydrophilic the results correspond with the findings of Ditscherlein et al. [25] who used atomic force microscopy (AFM) for the characterization of NBs on alumina substrates in water. They found hardly any bubbles on plane hydrophilic surfaces, but they showed that grooves and cavities of a hydrophilic surface are preferred sites for the formation of NBs as well. Nail et al. [26] also reported those surface defects as nucleation sites for bubbles on metallic surfaces.

Combining these results, it is concluded that the rough hydrophilic surface of Pt30 generated bulk NBs in the conducted pressure release experiments. The variations of the peak concentration of Pt30 particles in PSD (Fig. 4) were not systematically correlated with the pressurization visible as the overlapping of error bars at the Pt30 peak size. An increase in pressure followed by a venting step may result in an unchanged generation of bulk NBs. In addition, the non-constant concentration of platinum particles pointed to tearing-off mechanisms of NBs from the particle surface while venting the sample. Based on a dynamic model for bulk NBs as shown by Yasui et al. [27], NB-clusters with hydrophilic particles cannot exist stably in a suspension with surface-attached NBs unless a NB is fully covered with hydrophilic particles. This theory underlines the appearance of bulk NBs for gas treated hydrophilic Pt30 suspensions and implies that NBs might be responsible for inconsistency in platinum particle concentration. Hence, a detachment of formed NBs from the rough platinum particle surface is a realistic scenario since the cumulative particle concentration Q_0* increased with constant Pt30 particle size.

Regarding the Pt30 suspensions, which contained a small amount of ionic stabilizer (citrate), it was observed that a mixture of UPW with an equal concentration of citrate displayed the same behavior of NB formation as gas treated UPW. Thus, the citrate ions were not linked to the generation of NBs, as can be shown by NTA measurements (see Fig. 3).

3.3. Pressurization of smooth hydrophilic Au30 particles

As shown for rough platinum particles, dissolved gas molecules nucleated at grooves and cavities on particles' surface forming unattached bulk NBs. Assuming only the hydrophobicity/hydrophilicity to be relevant for bulk NB production, a smooth hydrophilic particle material is supposed to show a similar NB production effect. In order to prove the surface morphology to be relevant, smooth gold nanoparticles with 30 nm in diameter (Au30) were gas treated under the same conditions like Pt30 particles. The surface of those Au30 particles is shown in a TEM micrograph as an insert in Fig. 5, the PSDs of blank and gas treated Au30 suspensions and corresponding scatterplots are given as well.

Obviously, the gas treatment step neither affected the particle size of the gold particles nor the amount of bulk NBs. Only a few bulk NBs were measured for ambient gas treatment since the gas treated citrate showed some background effects. Belova et al. [28] indicated for ultrasonic cavitation experiments that only a hydrophobic aluminum surface was affected by cavitation bubbles. Untreated aluminum displayed no change due to the absence of ultrasonic induced bubbles. Therefore, as a result of gas treatment, it can be stated that a smooth hydrophilic metal surface, like Au30, did not produce surface attached NB or bulk NBs as can be seen in Fig. 5. By analyzing AFM images of titanium boundaries on silicon, Nishiyama et al. [29] found surface attached NBs on rather hydrophobic silicon but many NBs were identified in the vicinity of the hydrophilic titanium boundary close to silicon. Therefore it can be assumed that an edge of hydrophilic material is similar to a rough surface and enhances NB nucleation. Thus, concluding the gas treatment experiments, it can be summarized that for hydrophilic particle materials only the surface morphology is relevant

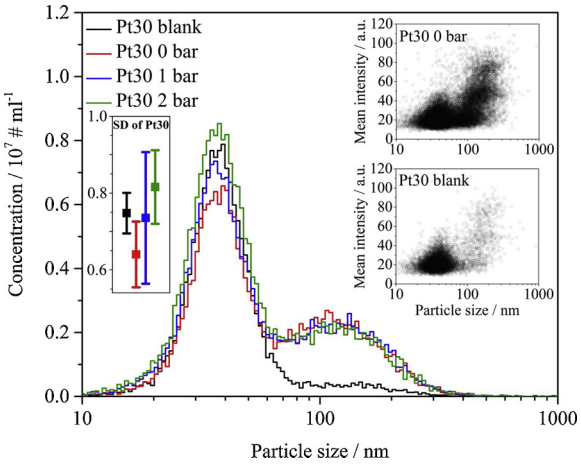

Fig. 4. Averaged PSDs (N_{rep} = 5) of Pt30 suspensions. Inserts: Standard deviation (SD) of Pt30 peak concentration at 36.1 nm and scatterplots of gas treated and blank Pt30 suspensions.

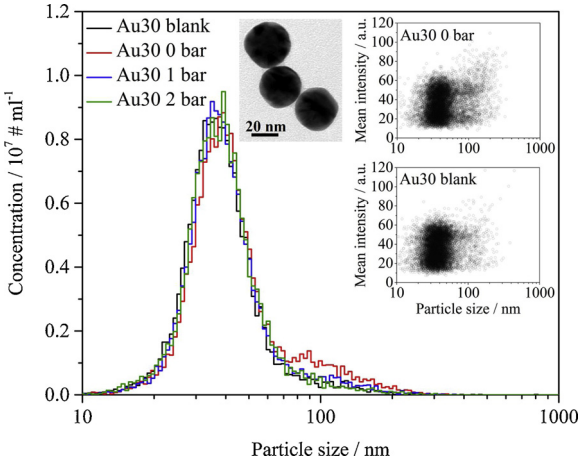

Fig. 5. Averaged PSDs (N_{rep} = 5) of Au30 suspensions. Inserts: TEM micrograph and scatterplots of gas treated and blank Au30 suspensions.

for NB production. For both sample series, Pt30 and Au30 respectively, the applied pressure had no effect on NB concentration.

3.4. Pressurization of smooth hydrophobic PS70 beads

The experiments discussed above were repeated using particles with substantially different surface properties. PS70 particles showed a hydrophobic, compact, and smooth surface with a spherical shape. As can be seen in Fig. 6, the gas treatment of PS70 particles shifted the whole particle size distribution to larger sizes without affecting the peak particle concentration. The averaged peak concentration of PS70 at 2 bar seemed decreased due to gas treatment. However, the standard deviation, represented as error marks, pointed to a non-systematical effect. The peak particle size was found to increase from 67.1 nm for the blank sample to 84.3 nm (arithmetic average for all gas treated suspensions from 0 bar–2 bar). The shift in the number based PSD seemed to be independent of the applied pressure and suggested a gradual increase. Yet, a doubling in cumulative volume distribution Q_3* (see Fig. 10, blank versus gas treated samples) of particle volume from $0.5 \times 10^{14}\,nm^3\,ml^{-1}$ to $1.0 \times 10^{14}\,nm^3\,ml^{-1}$ was observed. Agglomeration nor flocculation was observed in gas treated PS70 particle suspensions.

The scatterplots of gassed PS70 (inserts in Fig. 6) confirmed small changes to the pre-existing cloud of markers, but no significant appearance of bulk NBs. This is quite remarkable since the ionic surfactant (similar to SDS) used by the manufacturer showed some background effects in the pre-examination (cf. Fig. 3). Therefore it is concluded that the major part of the surfactant was adsorbed onto the particles' surface and gas nucleated only at the particles' surface. Presumably, due to the thin gas layer surrounding each particle, the surface attached NBs did not change the scatter signals of the ambient gas treated PS70 particles and the measured scattered light intensity can be analyzed as such from polystyrene.

Assuming that surfactant molecules are being adsorbed with their hydrophobic tail pointing towards the particles' surface, the PS particles might appear to be hydrophilic when looked at from a macroscopic point of view. In this case, the behavior of PS70 particles should be similar to those of hydrophilic Pt30 particles. A simple estimate based on SDS surface density experiments carried out by Pisárčik et al. [30] showed that even if all the surfactant molecules were attached to the particles, their surface would still not be fully covered. As discussed by Mitchell et al. [31], the geometric shape of the polar hydrophilic head group of a surfactant molecule is responsible for repulsive forces. As a result, the SDS molecules are assumed to be adsorbed with a certain distance to each other. Thus, spaces between the adjacent surfactant molecules may allow dissolved gas molecules to form NBs in the so formed hydrophobic patches, which together with the neighboring hydrophobic surfactant tails could be named "surfactant induced pores" of the particle. Following the experimental results in Fig. 6, they would be flooded with gas in an all-or-nothing process under any conditions, i.e. independent of the applied pressure in the conducted experiments. This assumption is supported by atomic force microscopy experiments by Fang et al. [32], who proved the existence of so-called *interfacial nanobubbles* on highly ordered pyrolytic graphite. Fang et al. stated that a surface-attached NB grows preferred in lateral size on a hydrophobic surface until an obstacle, i.e. a hydrophilic edge, is reached. Then, additional gas adsorption results in an increase in NB-height only. In the experiments described in this work, an adsorbed SDS molecule can be considered as such an obstacle that the bubble grew upwards resulting in an increased particle size (cf. Fig. 6). Consistent results were also reported by Ditscherlein et al. [25] and Knüpfer et al. [33] who found surface attached NBs on hydrophobized alumina substrates with AFM. In summary, it is concluded that, due to gas treatment, a hydrophobic PS surface and hydrophobic surfactant pores were able to form surface-attached NBs between adjacent stabilizer molecules without producing bulk NBs whereas the major effect with Pt30 is bulk NB production.

As a comparison to NTA size measurements of gas treated PS70 suspensions, a rough calculation of particle size based on geometrical assumptions should give a note to the validity of the sketch depicted in Fig. 7. Assuming the surface area of spherical PS70 particles covered with surfactant molecules, the number of adsorbed SDS molecules can be estimated to 15,394 based on a surface density of 1 nm^2 per SDS molecule [30] and a particle size of 70 nm. Then, the volume of the gas film around the solid particle (mentioned as surface-attached NBs) may be seen as the volume of a single surfactant induced pore multiplied by the number of adsorbed SDS molecules. It is critical to assume one SDS molecule to form one surfactant induced pore, here it was considered to be correct as a rough estimation. As a result, the volume of gas in terms of surface-attached NBs is 121,080.3 nm^3 and the volume-based recalculated particle size with surface-attached NBs is 83.1 nm. In comparison to 84.3 nm by NTA, a small error is apparent underlining the NTA measurements and the assumed appearance of surface-attached NBs (cf. Fig. 7) to be correct.

3.5. Binary mixture of Pt30 and PS70 particles

The described experimental work aimed at the development of a flotation process of the separation of nanomaterials. With respect to this, the observed differences in the behavior of Pt30 and PS70 particles

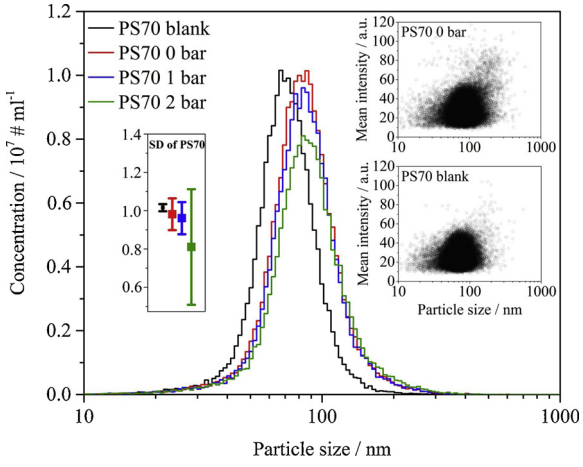

Fig. 6. Averaged PSDs (N_{rep} = 5) of PS70 suspensions. Inserts: Standard deviation (SD) of PS70 peak concentration at 67.1 nm for blank, and 83.3 nm for all gas treated suspensions and scatterplots of gas treated and blank PS70 suspensions.

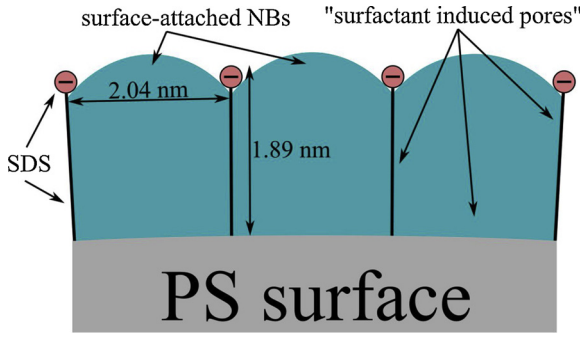

Fig. 7. Schematic of the PS70 particle surface with attached SDS molecules and gas-filled surfactant induced pores. Distances between adjacent SDS molecules and chain length in accordance with Pisárčik et al. [30].

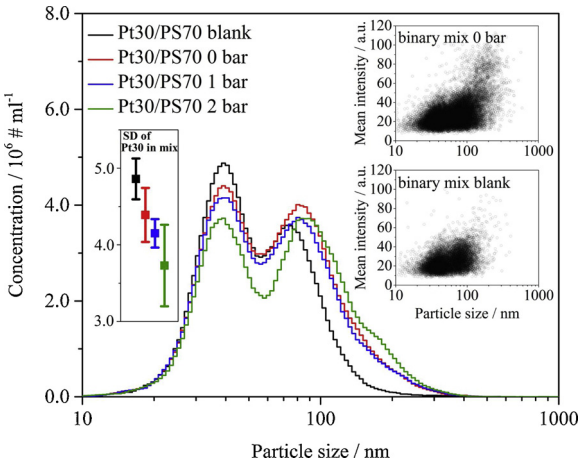

Fig. 8. Smoothed and averaged PSDs (N_{rep} = 5) of binary mixture Pt30/PS70. Inserts: Standard deviation (SD) of Pt30 peak concentration in binary mixtures at 39.1 nm and scatterplots of gas treated and blank Pt30/PS70 suspensions.

were encouraging. The hydrophilic particles would remain unchanged in size in a gas treated suspension while hydrophobic particles would acquire a lower overall density due to surface-attached NBs allowing for future separation in a centrifuge. It remained to be shown that the observed favorable results persist in gas treated binary mixtures of the materials. The blank suspension of Pt30 and PS70 as a mixture appeared stable without any separation or agglomeration.

Restrictively, this process assumes the NB-generation by platinum and an attachment mechanism of bulk NBs to PS surfaces. The interaction of bulk NBs with nanoparticles was discussed by Zhang et al. [16]. It was presumed that the collision of NBs with nanoparticles could not explain the growth in nanoparticle size after mixing NB-containing solution with nanoparticles. In fact, a re-nucleation of surface NBs caused by bulk NBs was proposed by Zhang et al.

Nevertheless, the gas treatment experiments of binary mixtures of Pt30 and PS70 particles provided good results which are in line with previous hypotheses. As shown in Fig. 8, the peak particle size of platinum particles appeared constant, even after gas treatment, which is consistent with former results of gas treatment of pure Pt30 particles (cf. Fig. 4). Only the PS70 peak shifted in the gas treated binary mixture towards larger sizes. Additionally, the right flanks of PSDs shifted as well. The extension of the right flanks in PSDs was correlated with the appearance of bulk NBs besides surface attached NBs. More counting events at larger particle sizes and higher mean intensities in scatterplots of gas treated suspensions also underlined the assumption of bulk NBs in gas treated binary mixtures.

For these experiments, the peak concentration of Pt30 particles in the binary mixture seemed to decrease with increasing pressure. A non-negligible standard deviation for Pt30 concentration in binary mixtures (error bars in Fig. 8) and their overlapping indicated the complexity of particle-bubble-mixtures with bulk and surface-attached NBs. Hence, from the decreased Pt30 concentration in a binary mixture, it cannot be stated precisely how the platinum behaved in the mixture.

However, two essential findings might be concluded from these gas treatment experiments: On the one hand, the shift in particle size for PS70 in binary mixture is in the same range as for purely gas treated PS70. So, the arithmetic average in peak particle size for gas treated pure PS70 (0 bar–2 bar) was 84.3 nm, 84.5 nm for PS70 in binary mixtures, respectively. The PS particles can be assumed to be flooded to

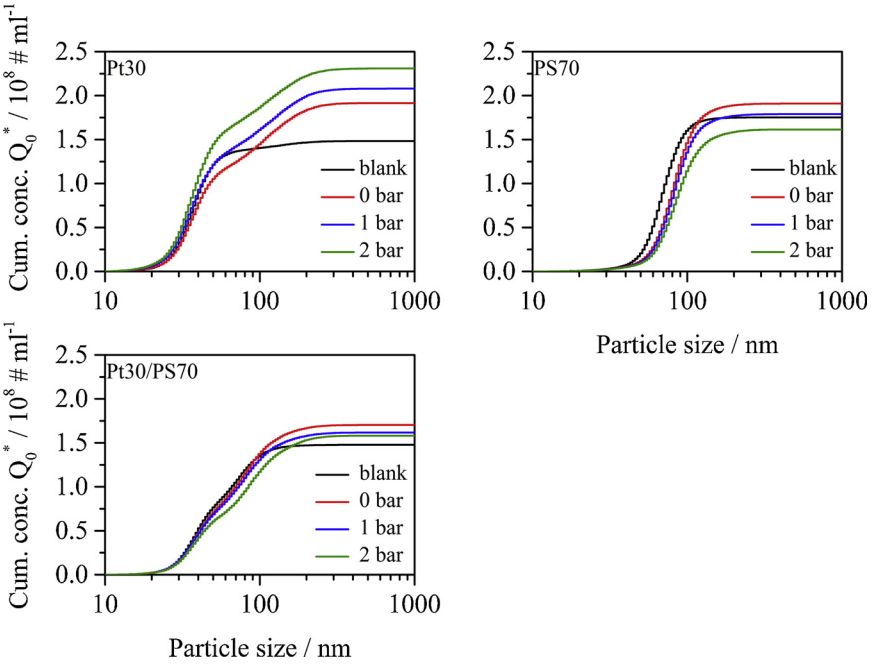

Fig. 9. Summary analysis of PSDs for Pt30, PS70 and binary mixture as cumulated particle concentration $Q_0^* = \sum_{i=1}^{n} C_{N,i}$ given in 10^8 # ml^{-1}.

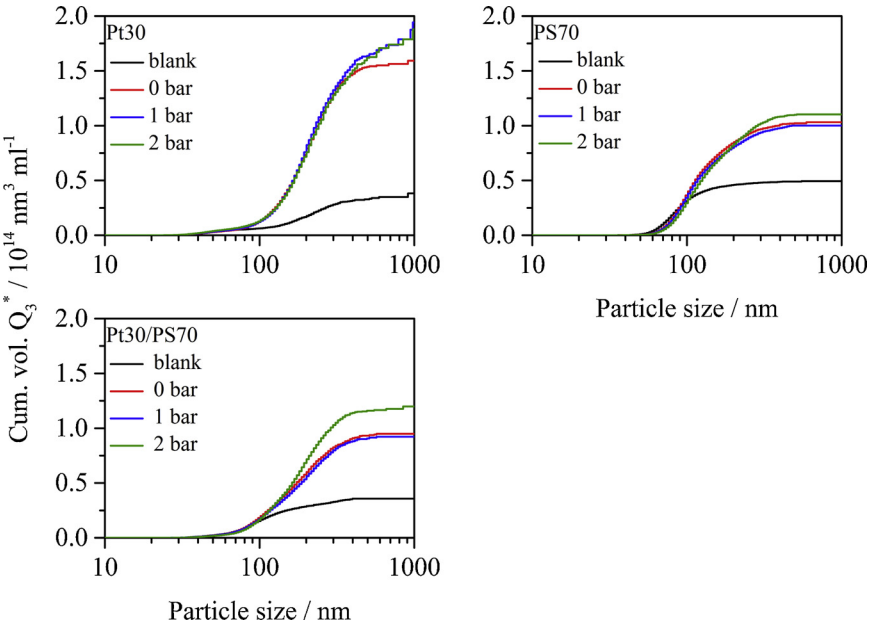

Fig. 10. Summary analysis of PSDs for Pt30, PS70 and binary mixture as cumulated particle volume $Q_3^* = \sum_{i=1}^{n} C_{N,i} \bullet V_{N,i}$ given in $10^{14}\,nm^3\,ml^{-1}$ with $V_{N,i} = \pi/6 \bullet d_{HD,i}^3$.

a maximum in pure and binary mixture experiments. Nevertheless, in more complex particle systems, i.e. under unsaturated conditions, the identified bulk NBs in binary mixtures could enhance a re-nucleation of gas onto particles without surface attached NBs as considered by Zhang et al. [16]. Thus, the appearance of bulk NBs in gas treated binary mixtures besides NB-attached PS may open up the chance of combining even more nanoparticles with NBs by a constant amount of platinum particles. On the other hand, the presented results have shown a binary particle system being changed that way, by gas treatment that the hydrophilic particle species remained unchanged in size and another hydrophobic one appeared modified. This selective change of a particle species allows separation in future processes because of the density modification caused by surface-attached NBs. The increase in cumulated particle volume Q_3^* (Fig. 10) for blank and pressurized (2 bar) Pt30/PS70 samples also demonstrated a significant change of the colloidal system in the meaning of free and surface-attached NBs. A first step towards a separation procedure was done with the modification of PS particles next to Pt30 particles. Further research is necessary in order to investigate proper separation methods for particle-bubble-clusters in future processes.

4. Conclusion

Based on gas treatment experiments of water-based suspensions containing hydrophilic and hydrophobic nanoparticles, it is concluded that the presence of particles extremely enhanced the formation of NBs. Rough hydrophilic platinum particles came up with a bimodal PSD after treatment, thus confirming particle surface-induced generation of free bulk NBs. In contrast, smooth hydrophobic polystyrene particles were found with NBs attached to their surface. Moreover, a shift in the particle size distribution was observed. Our first results on a gas treatment of a binary mixture of these particles showed that the size distribution obtained was, as might be expected as a first approximation, the linear combination of the individual results. Thus, in this model system, the key step towards a material-selective separation process of nanostructured materials by NBs has been demonstrated. These results will help to supplement NB- and MB-flotation experiments already carried out for micro-range particles [5,8] with flotation experiments on a nanometer scale. In contrast to investigations by Pourkarimi et al. [9] in our work, a pressure-release process without cavitation was demonstrated in which the usage of additives such as frother could be dispensed with, except stabilizer surfactants added by the particle manufacturers. The surface properties of a particle were found playing a central role in the flotation of nanoparticles by means of NB generation so that future investigations should focus on the influence of NB-formation, its attachment to a particle surface and a successful separation of particle-bubble-clusters.

CRediT authorship contribution statement

Vinzent Olszok: Formal analysis, Writing - original draft, Writing - review & editing, Visualization. **Juliana Rivas-Botero:** Investigation, Formal analysis. **Annett Wollmann:** Writing - review & editing, Supervision. **Bernd Benker:** Conceptualization, Writing - review & editing, Supervision. **Alfred P. Weber:** Funding acquisition, Project administration, Supervision.

Declaration of Competing Interest

The authors declare that they have no known competing financial interests or personal relationships that could have appeared to influence the work reported in this paper.

Acknowledgment

The authors would like to thank the German Research Foundation (DFG) for the financial support of the project DFG WE 2331/21-1 within the SPP 2045, and Mr. Johannes Fellner for preliminary investigations.

References

[1] S.H. Oh, J.M. Kim, Generation and stability of bulk nanobubbles, Langmuir 33 (2017) 3818–3823, https://doi.org/10.1021/acs.langmuir.7b00510.
[2] A.K.A. Ahmed, C. Sun, L. Hua, Z. Zhang, Y. Zhang, W. Zhang, T. Marhaba, Generation of nanobubbles by ceramic membrane filters: the dependence of bubble size and zeta potential on surface coating, pore size and injected gas pressure, Chemosphere 203 (2018) 327–335, https://doi.org/10.1016/j.chemosphere.2018.03.157.
[3] A. Azevedo, R. Etchepare, S. Calgaroto, J. Rubio, Aqueous dispersions of nanobubbles: generation, properties and features, Miner. Eng. 94 (2016) 29–37, https://doi.org/10.1016/j.mineng.2016.05.001.

[4] F.Y. Ushikubo, T. Furukawa, R. Nakagawa, M. Enari, Y. Makino, Y. Kawagoe, T. Shiina, S. Oshita, Evidence of the existence and the stability of nano-bubbles in water, Colloids Surfaces A Physicochem. Eng. Asp. 361 (2010) 31–37, https://doi.org/10.1016/j.colsurfa.2010.03.005.
[5] H. Kursun, U. Ulusoy, Zinc recovery from a lead-zinc-copper ore by ultrasonically assisted column flotation, Part. Sci. Technol. 33 (2015) 349–356, https://doi.org/10.1080/02726351.2014.970314.
[6] J.J. Royer, N. Monnin, N. Pailot-Bonnetat, L.O. Filippov, I.V. Filippova, T. Lyubimova, Thermodynamics of ultra-sonic cavitation bubbles in flotation ore processes, J. Phys. Conf. Ser. 879 (2017), https://doi.org/10.1088/1742-6596/879/1/012024.
[7] L. Falcon, The gravity recovery of cassiterite, J. South African Inst. Min. Metall. 82 (1982) 112–117.
[8] S. Calgaroto, A. Azevedo, J. Rubio, Flotation of quartz particles assisted by nanobubbles, Int. J. Miner. Process. 137 (2015) 64–70, https://doi.org/10.1016/j.minpro.2015.02.010.
[9] Z. Pourkarimi, B. Rezai, M. Noaparast, Effective parameters on generation of nanobubbles by cavitation method for froth flotation applications, Physicochem. Probl. Miner. Process. 53 (2017) 920–942, https://doi.org/10.5277/ppmp170220.
[10] W.B. Zimmerman, S. Butler, H. Bandulasena, Microbubble generation, Recent. Pat. Electr. Electron. Eng. E (2008), https://doi.org/10.2174/187221208783478598.
[11] A.A. Atchley, A. Prosperetti, The crevice model of bubble nucleation, J. Acoust. Soc. Am. 86 (1989) 1065–1084, https://doi.org/10.1121/1.398098.
[12] L. Liebermann, Air bubbles in water, J. Appl. Phys. 28 (1957) 205–211, https://doi.org/10.1063/1.1722708.
[13] R.E. Apfel, The role of impurities in cavitation-threshold determination, J. Acoust. Soc. Am. 48 (1970) 1179–1186, https://doi.org/10.1121/1.1912258.
[14] S.D. Lubetkin, D.J. Wedlock, Controlled particle, droplet and bubble formation, Oxford (1994).
[15] H. Kobayashi, S. Maeda, M. Kashiwa, T. Fujita, Measurement and identification of ultrafine bubbles by resonant mass measurement method, Int. Conf. Opt. Part. Charact. (OPC 2014) 9232 (2014) 92320S, https://doi.org/10.1117/12.2064811.
[16] M. Zhang, J.R.T. Seddon, Nanobubble-nanoparticle interactions in bulk solutions, Langmuir 32 (2016) 11280–11286, https://doi.org/10.1021/acs.langmuir.6b02419.
[17] V. Filipe, A. Hawe, W. Jiskoot, Critical evaluation of nanoparticle tracking analysis (NTA) by NanoSight for the measurement of nanoparticles and protein aggregates, Pharm. Res. 27 (2010) 796–810, https://doi.org/10.1007/s11095-010-0073-2.
[18] J. Panchal, J. Kotarek, E. Marszal, E.M. Topp, Analyzing subvisible particles in protein drug products: a comparison of Dynamic Light Scattering (DLS) and Resonant Mass Measurement (RMM), AAPS J. 16 (2014) 440–451, https://doi.org/10.1208/s12248-014-9579-6.
[19] L. Hu, Z. Xia, Application of ozone micro-nano-bubbles to groundwater remediation, J. Hazard. Mater. 342 (2018) 446–453, https://doi.org/10.1016/j.jhazmat.2017.08.030.
[20] M. Alheshibri, V.S.J. Craig, Generation of nanoparticles upon mixing ethanol and water; Nanobubbles or Not? J. Colloid Interface Sci. 542 (2019) 136–143, https://doi.org/10.1016/j.jcis.2019.01.134.
[21] Particle Metrix GmbH, PMX 120 Scanning ZetaView ® Lasermodul Technische Standarddaten, (2017).
[22] nanoComposix Inc, 30 nm Platinum Nanoparticles, Citrate, NanoXact, (2018).
[23] nanoComposix Inc, 30 nm Gold Nanospheres, Citrate, NanoXact, (2019).
[24] Thermo Fisher Scientific Inc., 3000 Series NanosphereTM Size Standards, https://www.thermofisher.com/order/catalog/product/3020A#/3020A (accessed September 23, 2019).
[25] L. Ditscherlein, J. Fritzsche, U.A. Peuker, Study of nanobubbles on hydrophilic and hydrophobic alumina surfaces, Colloids Surf. A Physicochem. Eng. Asp. 497 (2016) 242–250, https://doi.org/10.1016/j.colsurfa.2016.03.011.
[26] J.P. Nail, R.I. Vachon, J. Morehouse, An sem study of nucleation sites in pool boiling from 304 stainless steel, J. Heat Transfer 96 (1974) 132–137, https://doi.org/10.1115/1.3450152.
[27] K. Yasui, T. Tuziuti, W. Kanematsu, K. Kato, Dynamic equilibrium model for a bulk nanobubble and a microbubble partly covered with hydrophobic material, Langmuir 32 (2016) 11101–11110, https://doi.org/10.1021/acs.langmuir.5b04703.
[28] V. Belova, D.A. Gorin, D.G. Shchukin, H. Möhwald, Controlled effect of ultrasonic cavitation on hydrophobic/ hydrophilic surfaces, ACS Appl. Mater. Interfaces 3 (2011) 417–425, https://doi.org/10.1021/am101006x.
[29] T. Nishiyama, K. Takahashi, T. Ikuta, Y. Yamada, Y. Takata, Hydrophilic domains enhance nanobubble stability, ChemPhysChem 17 (2016) 1500–1504, https://doi.org/10.1002/cphc.201501181.
[30] M. Pisárčik, F. Devínsky, M. Pupák, Determination of micelle aggregation numbers of alkyltrimethylammonium bromide and sodium dodecyl sulfate surfactants using time-resolved fluorescence quenching, Open Chem. 13 (2015) 922–931, https://doi.org/10.1515/chem-2015-0103.
[31] D.J. Mitchell, B.W. Ninham, Micelles, vesicles and microemulsions, J. Chem. Soc. Faraday Trans. 2 Mol. Chem. Phys. 77 (1981) 601–629, https://doi.org/10.1039/F29817700601.
[32] C.K. Fang, H.C. Ko, C.W. Yang, Y.H. Lu, I.S. Hwang, Nucleation processes of nanobubbles at a solid/water interface, Sci. Rep. 6 (2016) 1–10, https://doi.org/10.1038/srep24651.
[33] P. Knüpfer, L. Ditscherlein, U.A. Peuker, Nanobubble enhanced agglomeration of hydrophobic powders, Colloids Surf. A Physicochem. Eng. Asp. 530 (2017) 117–123, https://doi.org/10.1016/j.colsurfa.2017.07.056.